Using Cyclooxygenase-2 Inhibitors as Molecular Platforms to Develop a New Class of Apoptosis-Inducing Agents

Jiuxiang Zhu, Xueqin Song, Ho-Pi Lin, Donn C. Young, Shunqi Yan, Victor E. Marquez, Ching-Shih Chen

Background: **The cyclooxygenase-2 (COX-2) inhibitor celecoxib is thought to act as a chemopreventive agent by sensitizing cancer cells to apoptotic signals. Other COX-2 inhibitors, such as rofecoxib, are two orders of magnitude less potent than celecoxib at inducing apoptosis. The molecular structures of celecoxib and rofecoxib were used as starting points to examine the structural features that contribute to this discrepancy.** ***Methods:*** **We used a systematic chemical approach to modify the structures of celecoxib and rofecoxib to produce a series of compounds that were tested for their effects on the viability of human prostate cancer PC-3 cells and their ability to induce apoptosis in these cells. Cell viability was measured by the trypan blue dye exclusion assay, and apoptosis was measured by an enzyme-linked immunosorbent assay that quantifies DNA cleavage and by western blot detection of poly(ADP-ribose) polymerase (PARP) cleavage. Western blotting was used to monitor the effects of the compounds on phosphorylation of the serine/threonine kinase Akt and extracellular signal-regulated kinase 2 (ERK2), two components of celecoxib-induced apoptosis signaling. Monte Carlo simulations were used to molecularly model the surface electrostatic potential and electron density of selected compounds. All statistical tests were two-sided.** ***Results:*** **The structural requirements for the induction of apoptosis in PC-3 cells were different from those for COX-2 inhibition. Structure–function analysis indicated that the induction of apoptosis by compounds derived from COX-2 inhibitors required a bulky terminal phenyl ring, a heterocyclic system with negative electrostatic potential, and a benzenesulfonamide or benzenecarboxamide moiety. These derivatives mediated apoptosis by facilitating the dephosphorylation of Akt and ERK2, irrespective of their COX-2 inhibitory activities.** ***Conclusion:*** **A new class of compounds that induce apoptosis by targeting Akt and ERK2 signaling pathways in human prostate cancer cells can be synthesized by modifying existing COX-2 inhibitors. [J Natl Cancer Inst 2002;94:1745–57]**

Results of recent epidemiologic and animal model studies have suggested that nonsteroidal anti-inflammatory drugs (NSAIDs) act as chemopreventive agents, especially for colon cancer *(1–9).* Several lines of evidence have attributed the antitumor activities of NSAIDs to their ability to sensitize cancer cells to apoptosis by blocking cyclooxygenase-2 (COX-2) enzyme activity *(10–13).* It is well documented that COX-2 is constitutively overexpressed in many types of human cancers and that decreased prostaglandin E_2 production as a result of COX-2 inhibition is associated with the modulation of various pro- and anti-apoptotic factors, such as Bcl-2 *(14),* prostate apoptosis-response gene (Par-4) *(15),* and caspase-3 *(16).* In addition, knockout of the COX-2 gene suppresses tumorigenesis in mice that have a genetic predisposition to form polyps *(17).* Recently, the U.S. Food and Drug Administration approved the use of the COX-2 inhibitor celecoxib for the adjuvant treatment of familial adenomatous polyposis, an inherited syndrome that predisposes individuals to colon cancer. In addition, celecoxib has also been tested in numerous clinical trials *(18)* for its chemopreventive effect on a variety of epithelial malignancies including colon, esophagus, skin, and bladder cancers.

However, an expanding body of evidence suggests that COX-2 inhibition may not play a role in NSAID-mediated apoptotic cell death *(19).* For example, sulindac sulfide and sulindac sulfone, which are metabolites of the NSAID sulindac, have been reported to mediate apoptosis in cancer cells via the inhibition of cyclic GMP phosphodiesterase *(20–23),* which is a COX-2-independent mechanism *(24).* In addition, we have used a tetracycline-inducible antisense COX-2 expression plasmid to demonstrate that the sensitivity of prostate cancer cells to COX-2 inhibitor-induced apoptosis is independent of the expression status of COX-2 *(25).* The finding that these two pharmacologic effects of NSAIDs—COX-2 inhibition and apoptosis induction—are separable has considerable therapeutic implications and provides molecular underpinnings for the design of a new class of anticancer compounds whose mode of action is different from that of conventional chemotherapeutic agents.

Celecoxib induces apoptosis in prostate cancer cells by interfering with multiple signaling targets, including the serine/threonine kinase Akt, extracellular signal-regulated kinase 2 (ERK2), and endoplasmic reticulum Ca^{2+}-ATPases *(26,27).* Disruption of these signaling pathways results in the loss of regulation of cellular functions that govern cell growth and survival, leading

Affiliations of authors: J. Zhu, H.-P. Lin (Division of Medicinal Chemistry and Pharmacognosy, College of Pharmacy), D. C. Young (Biostatistics Core, Comprehensive Cancer Center), The Ohio State University, Columbus; X. Song, Division of Pharmaceutical Sciences, College of Pharmacy, University of Kentucky, Lexington; S. Yan, V. E. Marquez, Laboratory of Medicinal Chemistry, Center for Cancer Research, National Cancer Institute at Frederick, Frederick, MD; C.-S. Chen, Division of Medicinal Chemistry and Pharmacognosy, College of Pharmacy, The Ohio State University, and Division of Pharmaceutical Sciences, College of Pharmacy, University of Kentucky.

Correspondence to: Ching-Shih Chen, Ph.D., College of Pharmacy, The Ohio State University, 336 Parks Hall, 500 W. 12th Ave., Columbus, OH 43210–1291 (e-mail: chen.844@osu.edu).

See "Notes" following "References."

to rapid apoptotic death. This rapid induction of apoptosis, however, is unique to celecoxib because other COX-2 inhibitors that have the same COX-2 inhibitory potencies as celecoxib, including rofecoxib (Vioxx®), NS398, and DuP697, display apoptosis-inducing activities that are nearly two orders of magnitude lower than that displayed by celecoxib *(26,27)*. Here we use celecoxib and rofecoxib as molecular starting points from which to understand the structural basis underlying this discrepancy and to optimize the apoptosis-inducing potency of celecoxib in prostate cancer cells.

Materials And Methods

Materials

Celecoxib and rofecoxib were extracted with ethyl acetate followed by recrystallization in a mixture consisting of ethyl acetate and hexane from Celebrex® and Vioxx®, respectively, which were obtained from Amerisource Health (Malvern, PA). NS398 was purchased from Calbiochem (San Diego, CA). Rabbit polyclonal antibodies against Akt, phospho-^{473}Ser Akt, p44/42 ERKs, and phospho-p44/42 ERKs were purchased from Cell Signaling Technologies (Beverly, MA). A rabbit polyclonal anti-poly(ADP-ribose) polymerase (PARP) antibody was obtained from Pharmingen (San Diego, CA). Other chemical and biochemical reagents used were obtained from Sigma-Aldrich (St. Louis, MO), unless otherwise mentioned.

Synthesis of Compounds

In this article, we discuss 50 compounds. The full chemical name of each of these compounds is provided in Table 1. We used published procedures to synthesize compounds **1, 1-NH$_2$, 2–29,** and **40–46.** *(28–31)*. Proton nuclear magnetic resonance

Table 1. List of compounds used in this study

Designation	Full chemical name
compound 1	1,2-difluoro-4-(4-fluorophenyl)-5-[4-(methylsulfonyl)phenyl]benzene
compound 1-NH$_2$	4-[4,5-difluoro-2-(4-fluorophenyl)phenyl]benzenesulfonamide
compound 2	4-[5-phenyl-3-(trifluoromethyl)-1*H*-pyrazol-1-yl]benzenesulfonamide
compound 3	4-[5-(4-fluorophenyl)-3-(trifluoromethyl)-1*H*-pyrazol-1-yl]benzenesulfonamide
compound 4	4-[5-(2,4-difluorophenyl)-3-(trifluoromethyl)-1*H*-pyrazol-1-yl]benzenesulfonamide
compound 5	4-[5-(2,5-difluorophenyl)-3-(trifluoromethyl)-1*H*-pyrazol-1-yl]benzenesulfonamide
compound 6	4-[5-(4-chlorophenyl)-3-(trifluoromethyl)-1*H*-pyrazol-1-yl]benzenesulfonamide
compound 7	4-[5-(2-chlorophenyl)-3-(trifluoromethyl)-1*H*-pyrazol-1-yl]benzenesulfonamide
compound 8	4-[5-(2,4-dichlorophenyl)-3-(trifluoromethyl)-1*H*-pyrazol-1-yl]benzenesulfonamide
compound 9	4-[5-(2,5-dichlorophenyl)-3-(trifluoromethyl)-1*H*-pyrazol-1-yl]benzenesulfonamide
compound 10	4-[5-(3,4-dichlorophenyl)-3-(trifluoromethyl)-1*H*-pyrazol-1-yl]benzenesulfonamide
compound 11	4-[5-(4-hydroxyphenyl)-3-(trifluoromethyl)-1*H*-pyrazol-1-yl]benzenesulfonamide
compound 12	4-[5-(4-aminophenyl)-3-(trifluoromethyl)-1*H*-pyrazol-1-yl]benzenesulfonamide
compound 13	4-[5-(4-nitrophenyl)-3-(trifluoromethyl)-1*H*-pyrazol-1-yl]benzenesulfonamide
compound 14	4-[5-(4-azidophenyl)-3-(trifluoromethyl)-1*H*-pyrazol-1-yl]benzenesulfonamide
compound 15	4-[5-(4-trifluoromethylphenyl)-3-(trifluoromethyl)-1*H*-pyrazol-1-yl]benzenesulfonamide
compound 16	4-[5-(4-cyanophenyl)-3-(trifluoromethyl)-1*H*-pyrazol-1-yl]benzenesulfonamide
compound 17	4-[5-(4-methoxyphenyl)-3-(trifluoromethyl)-1*H*-pyrazol-1-yl]benzenesulfonamide
compound 18	4-[5-(4-ethylphenyl)-3-(trifluoromethyl)-1*H*-pyrazol-1-yl]benzenesulfonamide
compound 19	4-[5-(2,4-dimethylphenyl)-3-(trifluoromethyl)-1*H*-pyrazol-1-yl]benzenesulfonamide
compound 20	4-[5-(2,5-dimethylphenyl)-3-(trifluoromethyl)-1*H*-pyrazol-1-yl]benzenesulfonamide
compound 21	4-[5-(3,4-dimethylphenyl)-3-(trifluoromethyl)-1*H*-pyrazol-1-yl]benzenesulfonamide
compound 22	4-[5-(2,4-dimethoxyphenyl)-3-(trifluoromethyl)-1*H*-pyrazol-1-yl]benzenesulfonamide
compound 23	4-[5-(2,5-dimethoxyphenyl)-3-(trifluoromethyl)-1*H*-pyrazol-1-yl]benzenesulfonamide
compound 24	4-[5-(2-pyridinyl)-3-(trifluoromethyl)-1*H*-pyrazol-1-yl]benzenesulfonamide
compound 25	4-[5-(1-cyclohexen-1-yl)-3-(trifluoromethyl)-1*H*-pyrazol-1-yl]benzenesulfonamide
compound 26	4-[5-(2-furanyl)-3-(trifluoromethyl)-1*H*-pyrazol-1-yl]benzenesulfonamide
compound 27	4-[5-(2-thienyl)-3-(trifluoromethyl)-1*H*-pyrazol-1-yl]benzenesulfonamide
compound 28	4-[5-(5-chloro-2-thienyl)-3-(trifluoromethyl)-1*H*-pyrazol-1-yl]benzenesulfonamide
compound 29	4-[5-(2,5-dichloro-3-thienyl)-3-(trifluoromethyl)-1*H*-pyrazol-1-yl]benzenesulfonamide
compound 30	4-[5-(4-chlorophenyl)-3-(trifluoromethyl)-1*H*-pyrazol-1-yl]benzenecarboxyamide
compound 31	4-[5-(2,4-dichlorophenyl)-3-(trifluoromethyl)-1*H*-pyrazol-1-yl]benzenecarboxyamide
compound 32	4-[5-(2,5-dichlorophenyl)-3-(trifluoromethyl)-1*H*-pyrazol-1-yl]benzenecarboxyamide
compound 33	4-[5-(3,4-dichlorophenyl)-3-(trifluoromethyl)-1*H*-pyrazol-1-yl]benzenecarboxyamide
compound 34	4-[5-(4-methylphenyl)-3-(trifluoromethyl)-1*H*-pyrazol-1-yl]benzenecarboxyamide
compound 35	4-[5-(4-trifluoromethylphenyl)-3-(trifluoromethyl)-1*H*-pyrazol-1-yl]benzenecarboxyamide
compound 36	4-[5-(4-ethylphenyl)-3-(trifluoromethyl)-1*H*-pyrazol-1-yl]benzenecarboxyamide
compound 37	4-[5-(2,4-dimethylphenyl)-3-(trifluoromethyl)-1*H*-pyrazol-1-yl]benzenecarboxyamide
compound 38	4-[5-(2,5-dimethylphenyl)-3-(trifluoromethyl)-1*H*-pyrazol-1-yl]benzenecarboxyamide
compound 39	4-[5-(3,4-dimethylphenyl)-3-(trifluoromethyl)-1*H*-pyrazol-1-yl]benzenecarboxyamide
compound 40	4-[5-(4-methylphenyl)-1*H*-pyrazol-1-yl]benzenesulfonamide
compound 41	4-[5-methyl-3-(4-methylphenyl)-4-isoxazolyl]benzenesulfonamide
compound 42	2-(4-methylphenyl)-5-(4-sulfamoylphenyl)thiophene
compound 43	4-[2,3-dihydro-3-(4-methylphenyl)-2-oxo-4-oxazolyl]benzenesulfonamide
compound 44	4-[2,3-dihydro-5-methyl-3-(4-methylphenyl)-2-oxo-4-oxazolyl]benzenesulfonamide
compound 45	4-[2,3-dihydro-3-(3,4-dichlorophenyl)-2-oxo-4-oxazolyl]benzenesulfonamide
compound 46	4-[2,3-dihydro-5-methyl-3-(3,4-dichlorophenyl)-2-oxo-4-oxazolyl]benzenesulfonamide
compound 47	3-(4-methylsulfonylphenyl)-4-phenyl-2(5*H*)-furanone
compound 48	3-(4-sulfamoylphenyl)-4-phenyl-2(5*H*)-furanone
compound 49	3-(4-sulfamoylphenyl)-4-(2,4-dichlorophenyl)-2(5*H*)-furanone
compound 50	3-(4-sulfamoylphenyl)-4-(3,4-dichlorophenyl)-2(5*H*)-furanone

(^{1}H NMR) spectroscopy, high-resolution mass spectrometry (HRMS), and elemental analysis were used to validate the identity of each of the synthetic compounds. The procedures we used to synthesize compounds **30–39** and **47–50** are presented below. Our results and the properties of these chemicals are summarized in Table 2.

4-[5-(4-Chlorophenyl)-3-(trifluoromethyl)-1*H*-pyrazol-1-yl] benzenecarboxyamide (compound **30**) was synthesized in two steps. In the first step, 4,4,4-trifluoro-1-(4-chlorophenyl)butane-1,3-dione was prepared as follows. To a solution of ethyl trifluoroacetate (1.08 g, 7.61 mmol) in 5 mL of methyl *tert*-butyl ether [MTBE] was added 25% sodium methoxide in methanol (1.8 mL) over a period of 2 minutes. A solution of 4′-chloroacetophenone (1 g, 6.46 mmol) in 2 mL of MTBE was then added to that mixture in a dropwise fashion over a period of 5 minutes. The resulting solution was stirred for 16 hours, 3 N HCl (3.4 mL) was added, and the aqueous and organic layers of the resulting mixture were allowed to separate. The organic layer was collected, washed with a saturated NaCl solution, dried over magnesium sulfate, and concentrated under vacuum in a rotary evaporator. The resulting yellow-orange solid was recrystallized from hexane, yielding 4,4,4-trifluoro-1-(4-chlorophenyl)butane-1,3-dione (1.18 g, 86% yield). In the second step, (4-carbamoylphenyl)hydrazine hydrochloride (228 mg, 1.21 mmol) was added to a stirred solution of the aforementioned dione (300 mg, 1.21 mmol) in 20 mL of ethanol. The resulting mixture was stirred under reflux for 24 hours, cooled to room temperature, and then concentrated to dryness under vacuum in a rotary evaporator. The resulting residue was dissolved in ethyl acetate, washed with a saturated NaCl solution, dried over magnesium sulfate, and concentrated under vacuum in a rotary evaporator. The resulting light brown solid was recrystallized from ethyl acetate and hexane to produce compound **30** (350 mg, 80% yield).

4-[5-(2,4-Dichlorophenyl)-3-(trifluoromethyl)-1*H*-pyrazol-1-yl]benzenecarboxyamide (compound **31**) was synthesized from 2′,4′-dichloroacetophenone using the two-step procedure described for the synthesis of compound **30,** in which 2′,4′-dichloroacetophenone was used in place of 4′-chloroacetophenone (52% overall yield).

4-[5-(2,5-Dichlorophenyl)-3-(trifluoromethyl)-1*H*-pyrazol-1-yl]benzenecarboxyamide (compound **32**) was synthesized from 2′,5′-dichloroacetophenone using the two-step procedure described for the synthesis of compound **30,** in which 2′,5′-dichloroacetophenone was used in place of 4′-chloroacetophenone (60% overall yield).

4-[5-(3,4-Dichlorophenyl)-3-(trifluoromethyl)-1*H*-pyrazol-1-yl]benzenecarboxyamide (compound **33**) was synthesized from 3′,4′-dichloroacetophenone using the two-step procedure described for the synthesis of compound **30,** in which 3′,4′-dichloroacetophenone was used in place of 4′-chloroacetophenone (55% overall yield).

4-[5-(4-Methylphenyl)-3-(trifluoromethyl)-1*H*-pyrazol-1-yl] benzenecarboxyamide (compound **34**) was synthesized from 4′-methylacetophenone using the two-step procedure described for the synthesis of compound **30,** in which 4′-methylacetophenone was used in place of 4′-chloroacetophenone (65% overall yield).

4-[5-(4-Trifluoromethylphenyl)-3-(trifluoromethyl)-1*H*-pyrazol-1-yl]benzenecarboxyamide (compound **35**) was synthesized from 4′-trifluoromethylacetophenone using the two-step procedure described for the synthesis of compound **30,** in which 4′-trifluoromethylacetophenone was used in place of 4′-chloroacetophenone (53% overall yield).

4-[5-(4-Ethylphenyl)-3-(trifluoromethyl)-1*H*-pyrazol-1-yl] benzenecarboxyamide (compound **36**) was synthesized from 4′-ethylacetophenone using the two-step procedure described for the synthesis of compound **30,** in which 4′-ethylacetophenone was used in place of 4′-chloroacetophenone (44% overall yield).

4-[5-(2,4-Dimethylphenyl)-3-(trifluoromethyl)-1*H*-pyrazol-1-yl]benzenecarboxyamide (compound **37**) was synthesized from 2′,4′-dimethylacetophenone using the two-step procedure described for the synthesis of compound **30,** in which 2′,4′-dimethylacetophenone was used in place of 4′-chloroacetophenone (62% overall yield).

4-[5-(2,5-Dimethylphenyl)-3-(trifluoromethyl)-1*H*-pyrazol-1-yl]benzenecarboxyamide (compound **38**) was synthesized from 2′,5′-dimethylacetophenone using the two-step procedure described for the synthesis of compound **30,** in which 2′,5′-dimethylacetophenone was used in place of 4′-chloroacetophenone (58% overall yield).

4-[5-(3,4-Dimethylphenyl)-3-(trifluoromethyl)-1*H*-pyrazol-1-yl]benzenecarboxyamide (compound **39**) was synthesized from 3′,4′-dimethylacetophenone using the two-step procedure described for the synthesis of compound **30,** in which 3′,4′-dimethylacetophenone was used in place of 4′-chloroacetophenone (56% overall yield).

3-(4-Methylsulfonylphenyl)-4-phenyl-2(5*H*)-furanone (compound **47**) was synthesized in two steps. In the first step, a mixture of 4′-(methylsulfonyl)acetophenone (5.5 g, 27.8 mmol), morpholine (2.5 mL), and sulfur (0.89 g, 27.8 mmol) was refluxed for 10 hours and then poured into ice where it formed a precipitate. The precipitate was collected by filtration and washed with cold ethyl acetate. The precipitate was added to 10% sodium hydroxide (55 mL), and the mixture was then heated to 84 °C for 12 hours, forming an alkaline solution that was acidified to pH 3 with 12 N HCl. The solid that resulted from acidification was collected by filtration, dried, and recrystallized from a solution containing equal volumes of hexane and ethyl acetate to give 4-methylsulfonylphenylacetic acid (a white solid; 4.2 g, 52% overall yield). In the second step, 2-bromoacetophenone (1.02 g, 5.12 mmol) dissolved in acetonitrile (28 mL) was added to triethylamine (1.74 mL), followed by the addition of 4-methylsulfonylphenylacetic acid (1 g, 4.67 mmol). The mixture was stirred at room temperature for 1.5 hours and then 1,8-diazabicyclo[5,4,0]undec-7-ene (1.67 mL) was added. The mixture was stirred for another hour, after which 1 N HCl (35 mL) was added. The end product was extracted from the mixture with ethyl acetate, dried over sodium sulfate, and recrystallized from ethyl acetate–hexane (vol/vol) to give compound **47** (880 mg, 60% overall yield).

3-(4-Sulfamoylphenyl)-4-phenyl-2(5*H*)-furanone (compound **48**) was synthesized from 4-sulfamoylphenylacetic acid and 2-bromoacetophenone in a manner similar to that described for compound **47,** with a 40% yield.

3-(4-Sulfamoylphenyl)-4-(2,4-dichlorophenyl)-2(5*H*)-furanone (compound **49**) was synthesized from 4-sulfamoylphenylacetic acid and 2-bromo-1-(2′4-dichlorophenyl)acetophenone in a manner similar to that described for compound **47,** with a 32% yield.

3-(4-sulfamoylphenyl)-4-(3,4-dichlorophenyl)-2(5*H*)-furanone (compound **50**) was synthesized from 4-sulfamoylphenylacetic acid and 2-bromo-1-(3′4-dichlorophenyl)acetophe-

Table 2. [1]H-NMR, high resolution mass spectrometry and elemental analysis data for compounds 30–39 and 47–50

Designation	Chemical shift, ppm*	Splitting pattern†	Coupling constant (J), Hz	No. of protons	Actual mass	Theoretical mass	Molecular formula	Actual composition, %	Theoretical composition, %
Compound 30	6.77	s	–	1	365.0522	365.0535	$C_{17}H_{11}ClF_3N_3O$	C = 55.72	C = 55.88
	7.16	d	8.4	2				H = 3.00	H = 3.04
	7.34	d	8.4	2				N = 11.45	N = 11.51
	7.40	d	8.4	2					
	7.83	d	8.4	2					
Compound 31	6.79	s	–	1	399.0138	399.0145	$C_{17}H_{10}Cl_2F_3N_3O$	C = 51.23	C = 51.13
	7.22	d	8.2	1				H = 2.76	H = 2.53
	7.27	d	8.2	1				N = 10.32	N = 10.53
	7.35	d	8.6	2					
	7.45	d	2.0	1					
	7.78	d	8.6	2					
Compound 32	6.79	s	–	1	399.0150	399.0145	$C_{17}H_{10}Cl_2F_3N_3O$	C = 49.99	C = 51.13
	7.37–7.40	m	–	5				H = 2.85	H = 2.53
	7.80	d	8.5	2				N = 10.16	N = 10.53
Compound 33	7.37	s	–	1	399.0162	399.0145	$C_{17}H_{10}Cl_2F_3N_3O$	C = 51.12	C = 51.13
	7.55	d	8.5	2				H = 2.76	H = 2.53
	7.66	d	8.5	2				N = 10.43	N = 10.53
	7.71	d	2.0	1					
	7.95	d	8.5	2					
Compound 34	2.37	s	–	3	345.1057	345.1081	$C_{18}H_{14}F_3N_3O$	C = 62.59	C = 62.48
	6.74	s	–	1				H = 4.31	H = 4.37
	7.10	d	8.2	2				N = 12.14	N = 12.24
	7.15	d	8.2	2					
	7.41	dd	1.8, 6.7	2					
	7.80	dd	1.8, 6.7	2					
Compound 35	7.45	s	–	1	399.0791	399.0798	$C_{18}H_{11}F_6N_3O$	C = 53.28	C = 54.12
	7.54	d	8.0	2				H = 2.98	H = 2.78
	7.62	d	8.0	2				N = 10.45	N = 10.52
	7.79	d	8.4	2					
	8.03	d	8.4	2					
Compound 36	1.24	t	7.6	3	359.1247	359.1238	$C_{19}H_{16}F_3N_3O$	C = 63.51	C = 63.49
	2.67	q	7.6	2				H = 4.67	H = 4.49
	6.74	s	–	1				N = 11.69	N = 11.70
	7.13	dd	2.2, 6.2	4					
	7.42	d	8.5	2					
	7.81	d	8.5	2					
Compound 37	1.94	s	–	3	359.1240	359.1238	$C_{19}H_{16}F_3N_3O$	C = 63.58	C = 63.49
	2.35	s	–	3				H = 4.88	H = 4.49
	6.65	s	–	1				N = 11.47	N = 11.70
	7.03	bs	–	1					
	7.08	d	8.2	2					
	7.35	d	8.6	2					
	7.73	d	8.6	2					
Compound 38	1.90	s	–	3	359.1268	359.1238	$C_{19}H_{16}F_3N_3O$	C = 63.59	C = 63.49
	2.32	s	–	3				H = 4.74	H = 4.49
	6.65	s	–	1				N = 11.57	N = 11.70
	7.08	m	–	3					
	7.36	d	8.5	2					
	7.73	d	8.5	2					
Compound 39	1.91	s	–	3	359.1257	359.1238	$C_{19}H_{16}F_3N_3O$	C = 63.57	C = 63.49
	2.34	s	–	3				H = 4.63	H = 4.49
	6.67	s	–	1				N = 11.67	N = 11.70
	7.08	m	–	3					
	7.36	d	8.5	2					
	7.73	d	8.5	2					
Compound 47	3.08	s	–	3	314.0632	314.0605	$C_{17}H_{14}O_4S$	C = 64.86	C = 64.96
	5.24	s	–	2				H = 4.61	H = 4.61
	7.18–7.30	m	–	5				N = 0	N = 0
	7.66	dd	1.9, 6.7	2					
	7.96	dd	1.9, 6.7	2					
Compound 48	5.43	s	–	2	315.0573	315.0557	$C_{16}H_{13}NO_4S$	C = 60.45	C = 60.94
	7.36–7.45	m	–	5				H = 4.29	H = 4.16
	7.76	d	8.5	2				N = 4.81	N = 4.44
	7.96	d	8.5	2					
Compound 49	5.42	s	–	2	382.9764	382.9778	$C_{16}H_{11}Cl_2NO_4S$	C = 49.22	C = 50.01
	7.26	dd	2.5, 8.5	1				H = 2.83	H = 2.89
	7.42	bs	–	1				N = 3.27	N = 3.65
	7.55	d	8.5	1					
	7.71	d	8.5	2					
	7.86	d	8.5	2					

(Table continues)

Table 2 (continued). [1]H-NMR, high resolution mass spectrometry and elemental analysis data for compounds 30–39 and 47–50

Designation	Chemical shift, ppm*	Splitting pattern†	Coupling constant (J), Hz	No. of protons	Actual mass	Theoretical mass	Molecular formula	Actual composition, %	Theoretical composition, %
Compound 50	5.42	s	–	2	382.9785	382.9778	$C_{16}H_{11}Cl_2NO_4S$	C = 50.31	C = 50.01
	7.26	dd	2.5, 8.5	1				H = 2.60	H = 2.89
	7.42	bs	–	1				N = 3.40	N = 3.65
	7.55	d	8.5	1					
	7.71	d	8.5	2					
	7.86	d	8.5	2					

*Compounds 33, 35, and 48–50 used DMSO-d_6 as a solvent in a 250MHz [1]H-NMR; all the other compounds used $CDCl_3$ as a solvent in a 250MHz [1]H-NMR. – = not applicable.

†The abbreviations s, bs, d, dd, t, q, m, and J used in describing [1]H-NMR parameters denote singlet, broad singlet, doublet, doublet doublet, triplet, quartet, multiplet, and coupling constant, respectively.

none in a manner similar to that described for compound **47,** with a 30% yield.

Cell Culture

The human prostate cancer cell lines LNCaP and PC-3 were purchased from the American Type Culture Collection (ATCC; Manassas, VA). Bcl-2-overexpressing PC-3 cells were prepared as previously described *(26).* Cells were cultured in RPMI-1640 medium (Gibco, Grand Island, NY) supplemented with 10% fetal bovine serum (FBS; Gibco) at 37 °C in a humidified incubator containing 5% CO_2. Cells were replenished daily with fresh medium and were harvested by trypsinization and split at a 1 : 4 ratio with fresh medium every 3 days.

Cell Viability Analysis

Prostate cancer cells were grown in 10% FBS-supplemented RPMI-1640 medium for 48 hours to approximately 60% confluency. The cells were then washed in serum-free RPMI-1640 and incubated in serum-free RPMI-1640 medium that contained various concentrations of celecoxib, rofecoxib, or test agent, each dissolved in 0.1% dimethyl sulfoxide (DMSO). Control cell cultures were washed in serum-free RPMI-1640 and then incubated in serum-free RPMI-1640 that contained the same concentration of DMSO as the celecoxib-treated cells. Floating cells were recovered from culture medium by centrifugation at 3200*g* for 5 minutes, and adherent cells were harvested by trypsinization. Both the floating and adherent cells were observed for morphologic changes with a light microscope at ×200 magnification. We combined the adherent and floating cells and measured their viability by using a trypan blue dye exclusion assay.

Assessment of Apoptosis

Enzyme-linked immunosorbent assay (ELISA) to detect DNA fragmentation. We used the Cell Death Detection ELISA kit (Roche Diagnostics, Mannheim, Germany), according to the manufacturer's instructions, to measure the induction of apoptosis in human prostate cancer cells treated with various compounds. This assay quantifies cytoplasmic histone-associated DNA fragments (both mono- and oligonucleosomes) that result from the induction of apoptosis. In brief, 2.5×10^6 PC-3 cells were plated in T-75 flasks and incubated for 24 hours. The cells were washed twice with 5 mL of serum-free RPMI-1640 medium and then incubated with serum-free medium containing the test compounds as described above. We then collected and pooled the floating and adherent cells, as described above, and counted them. Cell lysates equivalent to 10^4 cells were used for the ELISA analysis. Histone-associated DNA fragments were quantitated spectrophotometrically using antibodies against DNA and histones in a colorimetric assay.

Western blot analysis of PARP cleavage. PC-3 cells treated with DMSO or the various compounds as described above were collected, washed with ice-cold phosphate-buffered saline (PBS), and resuspended in 50 μL of lysis buffer (20 m*M* Tris–HCl [pH 8], 137 m*M* NaCl, 1 m*M* $CaCl_2$, 10% glycerol, 1% Nonidet P-40, 0.5% deoxycholate, 0.1% sodium dodecyl sulfate (SDS), 100 μ*M* 4-(2-aminoethyl)benzenesulfonyl fluoride, 10 μg/mL leupeptin, and 10 μg/mL aprotinin) for 10 minutes. Soluble cell lysates were collected after centrifugation at 1500*g* for 5 minutes. Protein concentrations of the lysates were determined by using a Bradford protein assay kit (Bio-Rad, Hercules, CA); equivalent amounts of protein from each lysate were resolved in 10% SDS–polyacrylamide gels and then transferred to nitrocellulose membranes. Western blotting with an anti-PARP antibody was carried out as described below, and apoptosis was detected by monitoring proteolysis of the 116-kd native PARP enzyme to the apoptosis-specific 85-kd fragment.

Western Blot Analysis of Apoptosis Signaling Components

Treated cells collected as described above, washed with PBS, resuspended in SDS gel-loading buffer (100 m*M* Tris–HCl [pH 6.8], 4% [wt/vol] SDS, 0.2% [wt/vol] bromophenol blue, 20% [vol/vol] glycerol, and 200 m*M* dithiothreitol), sonicated with an ultrasonic sonicator for 5 seconds, and boiled for 5 minutes. After brief centrifugation, equivalent amounts of soluble protein, as determined by the Bradford method, were resolved in 10% SDS–polyacrylamide minigels and transferred to nitrocellulose membranes with the use of a semidry transfer cell (Bio-Rad). The membranes were washed twice with TBS (0.3% [wt/vol] Tris, 0.8% [wt/vol] NaCl, and 0.02% [wt/vol] KCl) containing 0.05% Tween 20 (TBST) and then incubated with TBS containing 5% nonfat dry milk for 60 minutes to block nonspecific antibody binding. Each membrane was then incubated at 4 °C for 12 hours with a primary antibody specific for Akt, phospho-Akt, ERKs, phospho-ERKs, or PARP, which was diluted 1 : 1000 in TBS containing 1% nonfat dry milk. The membranes were washed twice with TBST and then incubated at room temperature for 1 hour with a horseradish peroxidase-conjugated goat anti-rabbit immunoglobulin G (IgG) diluted 1 : 5000 in TBS containing 1% nonfat dry milk. The membranes were washed twice with TBST, and bound antibody was visualized by enhanced chemiluminescence using ECL™ western blotting detection reagents (Amersham Pharmacia Biotech, Little Chalfont, U.K.). Unphosphorylated Akt and ERK2, as immunostained by anti-

Akt and anti-ERK2 antibodies, were used as internal standards for the comparison of phospho-Akt and phospho-ERK2 levels among samples of different exposure intervals.

Molecular Modeling Experiments

Molecular structures of compounds **47–50,** as well as celecoxib and rofecoxib, were initially subjected to 1000 steps of Monte Carlo simulation using the Merck Molecular Force Field program available as part of Macromodel 7.0 (Schrodinger, Portland, OR; http://www.schrodinger.com). The minimum conformation reached by the Monte Carlo simulations was then fully optimized at a density functional theory level of B3LYP/6–31G* with Gaussian 98A7 (Gaussian, Inc., Pittsburgh, PA) *(32).* All the fully optimized structures were confirmed by normal mode analysis; no negative frequencies were found. Computations for electrostatic potential and electron density were then carried out for each of the fully optimized structures with a grid of 216 000 points using Gaussian 98A7. The electrostatic potential maps for each compound were generated by gOpenMol (http://staff.csc.fi/~laaksone/gopenmol/gopenmol.html) *(33,34)* and are presented with the electrostatic potential mapped onto the electron density. The electron density isosurface value was 0.0004 with a range of –0.03 to 0.03 for the electrostatic potential.

Statistical Analysis

Each experiment was performed in triplicate and was repeated at least two times on different occasions. Analyses included nonparametric and parametric techniques to include analysis of variance (ANOVA) for linear models of dose response, ANOVA with Scheffé *post hoc* comparisons, Kruskal–Wallis nonparametric ANOVA, and Spearman rank correlation. A two-sided alpha of 0.05 was considered statistically significant.

We used two descriptive terms—the $T_{50\%}$ and the apoptosis index—to express the apoptosis-inducing activity of individual compounds in PC-3 cells. $T_{50\%}$ denotes the time required for eliciting apoptotic death in 50% of the cells when they are exposed to a specific concentration of the test compound. The apoptosis index is a semiquantitative indication of the apoptosis-inducing activity of a compound and was defined according to the $T_{50\%}$ for cells exposed to test compound at 50 μM. Compounds were classified into the following four categories of apoptosis index (in descending order of apoptosis-inducing activity): +++, $T_{50\%}$ is less than or equal to 2 hours; ++, $T_{50\%}$ is greater than 2 hours but less than or equal to 4 hours; +, $T_{50\%}$ is greater than 4 hours but less than or equal to 24 hours; and −, induced no appreciable apoptosis at 24 hours. Cut points to define the categories of apoptosis indices were determined by first performing ANOVA for all $T_{50\%}$ values for the compounds that elicited an apoptotic effect. Although there were statistically significant differences in apoptosis index among the different compounds ($P<.001$), no differences were seen among LNCaP, PC-3, and Bcl-2-overexpressing PC-3 cells ($P = .49$). To simplify the identification of the apoptosis index categories, we separated groups of compounds into those that had an apoptosis index of 2 hours or less and those that had an apoptosis index of greater than 2 hours, using the rounded group midpoint value of 2 hours that was determined from a conservative Scheffé *post hoc* comparison. Because compounds were evaluated in all three cell lines only at a dose of 50 μM, no dose–response relationship was analyzed.

The purpose of using these two descriptive terms was twofold. First, these two parameters, along with the IC_{50} (concentration for 50% inhibition) for COX-2 inhibition, allowed us to confirm our previous finding that COX-2 inhibition and apoptosis induction were independent. Second, the use of these terms allowed us to identify compounds that had high apoptosis-inducing potencies.

Results

Chemistry and Overall Strategy

The objective of this structure–function analysis of celecoxib and rofecoxib was twofold: to elucidate the structural basis underlying the discrepancy in apoptosis-inducing potency between the COX-2 inhibitors celecoxib and rofecoxib and to optimize the activity of celecoxib with regard to apoptosis induction. To attain these goals, we systematically altered the structure of celecoxib using the strategies to modify the moieties depicted in Fig. 1, A. In strategy A, we either modified the terminal aromatic ring of celecoxib with various substituents to produce compounds **2–23,** or replaced the terminal aromatic ring with different ring systems to produce compounds **24–29** (*see* Fig. 3 for structures). In strategy B, we substituted the carboxamide group for the sulfonamide group of various apoptosis-active celecoxib derivatives to produce compounds **30–39** (*see* Fig. 5 for structures). In strategy C, we modified the heterocyclic system of celecoxib to produce compounds **40–46** (Fig. 1, B). Molecular structures of celecoxib and rofecoxib were also subjected to computer modeling to examine the effect of surface potential on apoptosis; compounds **47–50** were prepared, on the basis of computer modeling of those compounds (*see* Fig. 1, B, and 6, C, for structures).

All compounds were evaluated for their ability to induce apoptotic cell death in human prostate cancer PC-3 cells, which are androgen-independent and deficient in p53 expression. Compounds that induced apoptosis in PC-3 cells were further evaluated for their ability to induce apoptosis in two additional cell lines—human prostate cancer LNCaP cells, which are androgen-dependent and express wild-type levels of p53, and Bcl-2-overexpressing PC-3 cells *(26).* For each compound tested, the $T_{50\%}$ value and apoptosis index obtained in each of the three cells lines were similar, indicating that the induction of apoptosis was not dependent on androgen sensitivity, p53 functional status, or the level of Bcl-2 expression. We therefore present cell viability and apoptosis data only for studies performed using PC-3 cells.

Role of the Sulfamoyl Moiety of Celecoxib in the Induction of Apoptosis

We tested COX-2 inhibitors that have similar IC_{50} values for COX-2 inhibition for their apoptosis-inducing activities in PC-3 cells and found that these COX-2 inhibitors exhibited widely discrepant apoptosis-inducing activities (Fig. 2, A). On the basis of their respective apoptosis indices (AIs) in PC-3 cells, we classified these COX-2 inhibitors into two groups—those that induced apoptosis (e.g., celecoxib) and those that did not (e.g., rofecoxib, NS398, DuP697, and the terphenyl deriva-

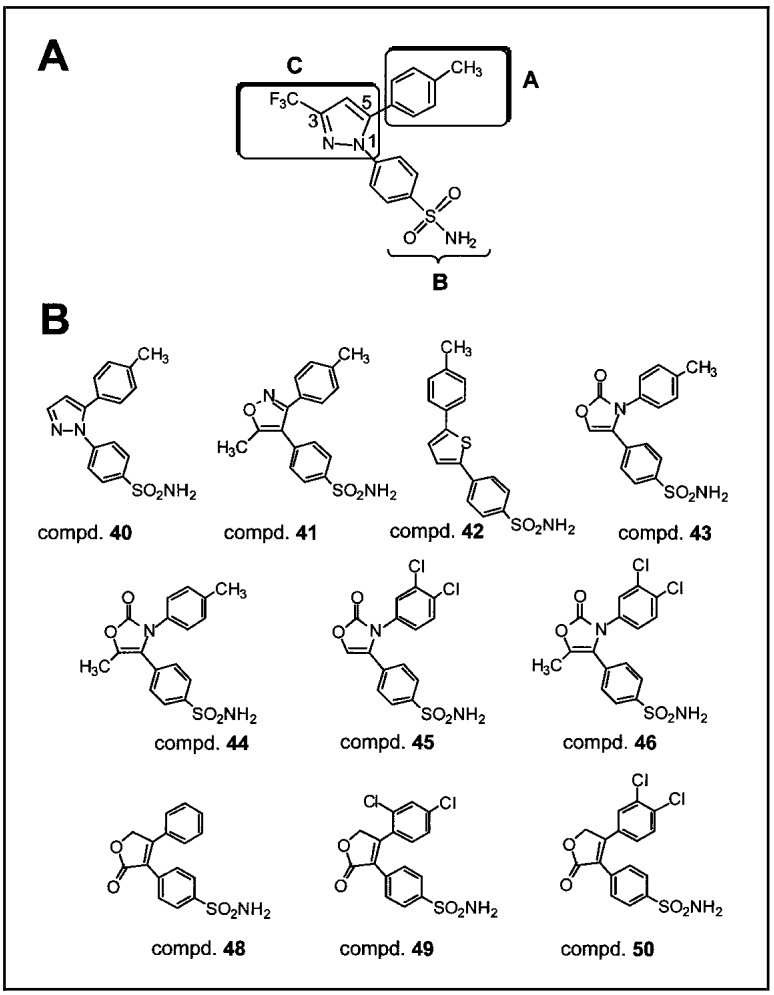

Fig. 1. Structure of celecoxib and some derivatives. **A**) Overall strategy for the structural modification of celecoxib. **A, B,** and **C** denote the three modification strategies that target the terminal phenyl ring, the sulfonamide group, and the heterocyclic system, respectively. The numbers **1, 3,** and **5** indicate the position of substituents on the pyrazole ring. **B**) Chemical structures of compounds **40–46** and **48–50.**

tive of DuP697, compound **1**) (Fig. 2). Structurally, these COX-2 inhibitors could be classified into two groups according to the type of sulfonyl (-SO_2-) functionality they contained, i.e., sulfonamide (-SO_2NH_2) or methylsulfone (-SO_2CH_3). As shown in Fig. 2, A, celecoxib contains a sulfonamide group, whereas rofecoxib, NS398, DuP697, and compound 1 all contain a methylsulfone group. This structural difference suggests that the sulfamoyl moiety of celecoxib may play a role in its apoptosis-inducing activity. This possibility was strengthened by our demonstration that the methylsulfone-containing counterpart of celecoxib was a less potent inducer of apoptosis than celecoxib (Fig. 2, B, left panel). Moreover, modification of compound **1** to compound **1-NH_2** *(28)* resulted in an increase in apoptosis-inducing activity by an order of magnitude (Fig. 2, B, right panel). The conversion of rofecoxib and DuP697 to their sulfonamide counterparts, however, did not substantially affect the apoptosis-inducing activities of those compounds (data not shown), indicating that structural elements other than the sulfonamide group contributed to the activation of the apoptosis machinery by celecoxib and compound **1-NH_2**.

Effect of the Terminal Phenyl Ring on the Apoptosis-Inducing Activity of Celecoxib

We synthesized a series of celecoxib derivatives (i.e., compounds **2–29**) to assess the role of the terminal phenyl ring on the apoptosis-inducing activity of celecoxib (Fig. 3). We found that the structural requirements for the induction of apoptosis by these compounds included a certain degree of bulkiness and hydrophobicity in the 5-aryl ring and were distinct from those required for COX-2 inhibition *(29).* For example, when we reduced the size of the 5-aryl ring (i.e., from a CH_3 group in celecoxib to an H group in compound **2** or an F group in compound **3**) or increased its polarity (e.g., from a CH_3 group to an OH group in compound **11,** an NH_2 in compound **12,** or an NO_2 group in compound **13**), the apoptosis indices of the resulting compounds decreased precipitously. Among the 28 derivatives we examined, compounds **8, 10, 14,** and **19–21** had an apoptosis index of +++ in PC-3 cells; compounds **6, 7, 9, 15,** and **18** had an apoptosis index of ++; and the remaining compounds displayed no appreciable apoptosis induction at 24 hours (i.e., an apoptosis index of −).

Celecoxib induces apoptosis by a mechanism that involves the concomitant dephosphorylation of Akt and ERK2 *(25–27).* We therefore examined whether the compounds with the most potent apoptotic indices induced cell death by a mechanism similar to that of celecoxib. Fig. 4, A, depicts the time- and/or dose-dependent effects of one of the active compounds generated by strategy A, compound **10,** on cell viability. ELISA analysis of the lysates from drug-treated cells revealed the time-dependent formation of oligonucleosomes as a result of DNA degradation (Fig. 4, B, left panel). In addition, immunoblot analysis of PARP indicated that exposure of PC-3 cells to compound **10** led to the rapid cleavage of the 116-kd native enzyme to form the apoptosis-specific 85-kd fragment (Fig. 4, B, right

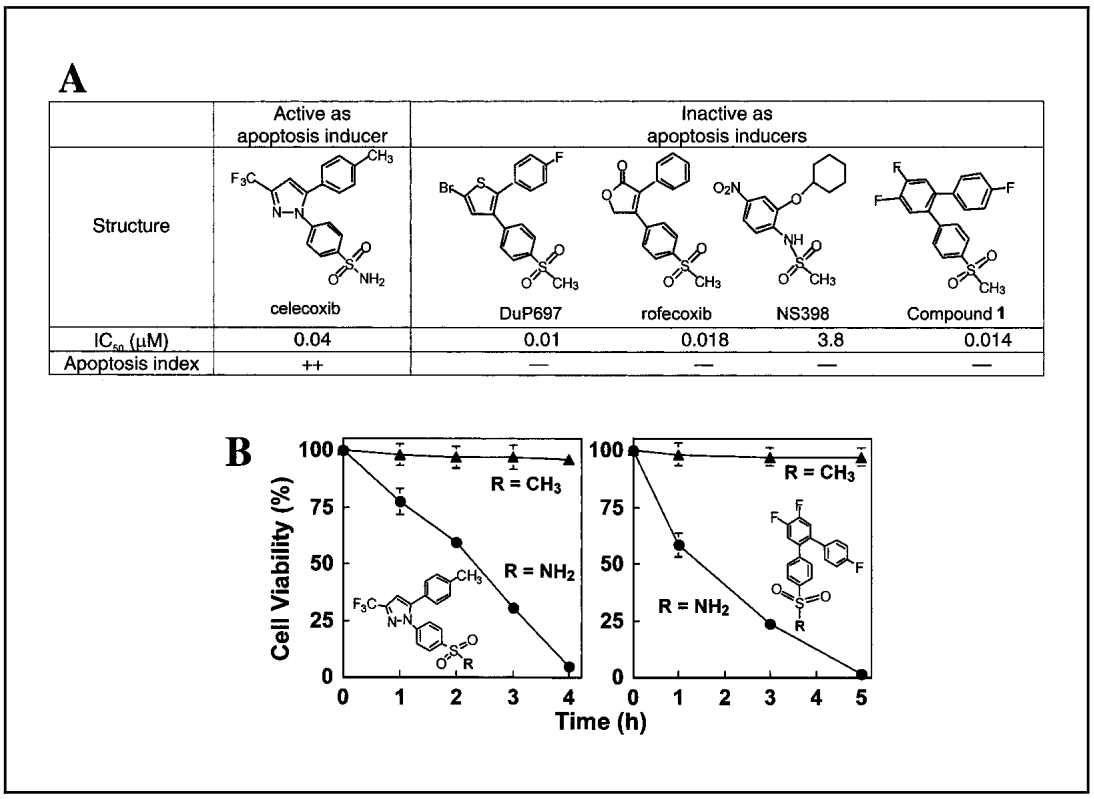

Fig. 2. Effect of sulfonamide versus methylsulfone on the apoptosis-inducing activity of various COX-2 inhibitors in PC-3 cells. **A**) Structures, IC_{50} values for COX-2 inhibition, and apoptosis indices of various COX-2 inhibitors. PC-3 cells were exposed to the test agent (50 μ*M*) in serum-free RPMI-1640 medium to assess the effects of the agent on apoptosis. IC_{50} represents the concentration required to inhibit 50% of the COX-2 enzyme activity. The apoptosis index was determined as described in the "Materials and Methods" section. **B**) Comparison of the effects of sulfonamide versus methylsulfone pharmacophores on cell viability. Cell viability was analyzed by the trypan blue dye exclusion assay. **Left panel,** celecoxib (R = NH_2) and its methylsulfone counterpart (R = CH_3); **right panel,** compound **1** (R = CH_3) and compound **1-NH$_2$** (R = NH_2). Data are presented as the mean values of three experiments; **bars** represent 95% confidence intervals.

panel). It is also noteworthy that the mechanism by which compound **10** caused apoptosis, i.e., dephosphorylation of Akt and ERK2 (Fig. 4, C), was the same as that by which celecoxib causes apoptosis. Similar results were obtained with other active compounds in this group. The dose–response relationship for compound **10,** with respect to cell viability, was statistically significant (ANOVA, $P<.001$ for time, dose, and cell viability). Fig. 4, B, shows that PC-3 cells treated with compound **10** displayed statistically significantly higher levels of ELISA-detectable nucleosome formation, an indicator of apoptotic cell death, over time than did PC-3 cells treated with DMSO (ANOVA; $P<.001$; mean readings [n = 3] at OD_{450} at 10, 20, and 30 minutes were 2.6 [95% CI = 2.5 to 2.7], 4.1 [95% CI = 4.0 to 4.2], and 4.1 [95% CI = 4.0 to 4.2], respectively, for drug-treated cells and 0.21 [95% CI = 0.18 to 0.24], 0.22 [95% CI = 0.20 to 0.24], and 0.16 [95% CI = 0.15 to 0.17], respectively, for DMSO-treated cells.

Because many of the compounds generated by strategy A are potent COX-2 inhibitors *(29),* we evaluated the relationship between COX-2 inhibition and induction of apoptosis by performing a nonparametric Spearman rank correlation analysis of the IC_{50} values of these compounds and the time they took to achieve a 50% reduction in cell viability at a concentration of 50 μ*M*. We found no correlation ($P = .44$). A similar nonparametric Kruskal–Wallis test showed no differences in the IC_{50} values among compounds in the four apoptosis index groups ($P = .67$). Although some compounds displayed high potency in inducing apoptosis, they lacked substantial COX-2 inhibitory activity and vice versa. This lack of correlation between apoptosis induction and COX-2 inhibition was consistent with our preliminary data *(25)* and confirmed that these two pharmacologic activities could be separated.

Apoptosis-Inducing Activities of Celecoxib Analogues That Contain a Carboxamide Moiety in Place of the Sulfamoyl Moiety

Although both the sulfonamide and methylsulfone pharmacophores showed comparable potency in COX-2 inhibition *(29),* the apoptosis-inducing activity of celecoxib was abrogated when the sulfamoyl moiety was replaced by a methylsulfonyl group. The result suggested that the sulfonamide pharmacophore conferred optimal potency with regard to apoptosis induction. We further investigated whether this functional group could be replaced by a carboxamide moiety without abrogating apoptosis-inducing activities of the resulting compounds. Accordingly, we determined the apoptosis indices for compounds **30–39,** which possess a carboxamide group in place of the sulfonamide group present in compound **6,** compounds **8–10,** celecoxib, compound **15,** and compounds **18–21.** As shown in Fig 5, A, replacement of the sulfonamide group in compounds **8, 9, 10,** and **19** with a carboxamide group to produce compounds **31, 32, 33,** and **37,** respectively, had no substantial effect on the potency of the resulting compounds in apoptosis induction. However, for the rest of the compounds examined (i.e., compounds **30, 34, 35, 36, 38,** and **39**), the replacement of the sulfonamide group with a carboxamide group resulted in a substantial reduction in their apoptosis-inducing activities. This observation suggested that these two pharmacophores (i.e., carboxamide and sulfonamide) may cause some compounds that contain them to interact differently with the target protein(s) that affect apoptosis. With compound **37** as a representative of this class of derivatives, Fig. 5, B, shows evidence of drug-induced apoptotic death, which included time-dependent effects on nucleosomal formation (treated versus control, ANOVA, $P<.001$) and PARP cleavage. Moreover, the structural modification of compound **19** to com-

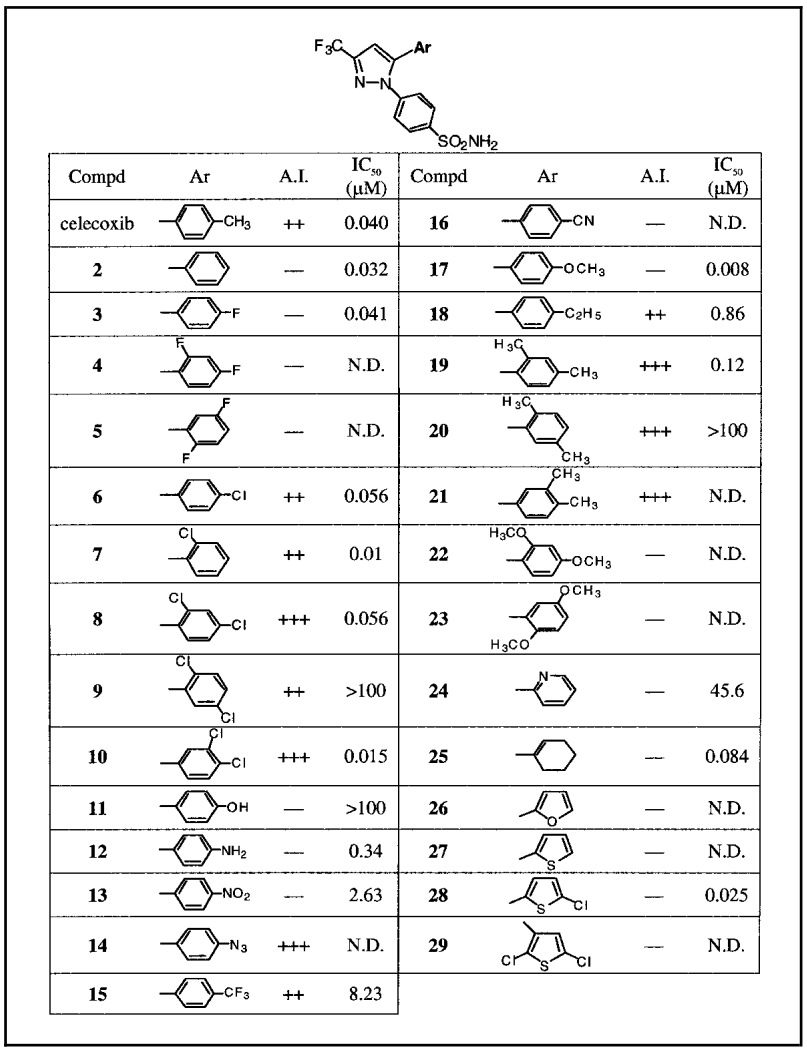

Compd	Ar	A.I.	IC_{50} (μM)	Compd	Ar	A.I.	IC_{50} (μM)
celecoxib		++	0.040	**16**		—	N.D.
2		—	0.032	**17**		—	0.008
3		—	0.041	**18**		++	0.86
4		—	N.D.	**19**		+++	0.12
5		—	N.D.	**20**		+++	>100
6		++	0.056	**21**		+++	N.D.
7		++	0.01	**22**		—	N.D.
8		+++	0.056	**23**		—	N.D.
9		++	>100	**24**		—	45.6
10		+++	0.015	**25**		—	0.084
11		—	>100	**26**		—	N.D.
12		—	0.34	**27**		—	N.D.
13		—	2.63	**28**		—	0.025
14		+++	N.D.	**29**		—	N.D.
15		++	8.23				

Fig. 3. Apoptosis induction and COX-2 inhibition data for celecoxib and compounds **2–29.** The general structure of these molecules is shown at the top. Ar represents different aromatic ring structures contained on the compounds. The apoptosis index (AI) was determined as described in the "Materials and Methods" section. IC_{50} represents the concentration required to inhibit 50% of the COX-2 enzyme activity; IC_{50} values were taken from *(29).* N.D. = not determined.

pound **37** did not alter the mechanism by which this carboxamide-containing compound mediated apoptosis, i.e., by facilitating Akt and ERK2 dephosphorylation (Fig. 5, C). Similar results were obtained with the other active compounds in this group.

Contributions of the Heterocyclic System to the Apoptosis-Inducing Activity of Celecoxib

The sulfonamide-containing counterparts of rofecoxib and DuP697 did not show substantial apoptosis-inducing activities in PC-3 cells (data not shown). This finding indicated that structural components other than the sulfonamide group may play a role in interacting with the target protein(s) responsible for apoptosis. To shed light on this issue, we further examined the effect of a number of benzenesulfonamides with different heterocyclic rings (i.e., compounds **40–46**) on the viability of PC-3 cells. Despite the presence of the sulfonamide group, none of these compounds displayed appreciable apoptosis induction at 24 hours (data not shown). Both replacement of the pyrazole ring with other heterocyclic systems and removal of the trifluoromethyl moiety from the pyrazole ring of celecoxib eliminated the apoptosis-inducing activity of the resulting compounds. This finding indicates the effect of the heterocyclic system on the apoptosis-inducing activity.

Molecular Modeling

The above data prompted us to examine how the heterocyclic ring might contribute to the interaction of celecoxib with the signaling target(s) responsible for apoptosis. We therefore conducted a molecular modeling analysis of the two prototypic drugs celecoxib and rofecoxib to examine the electrostatic potentials that surround the heterocyclic systems in these compounds (Fig. 6, A and B). The electron density of individual areas is colored blue to indicate negative electrostatic potentials and red to indicate positive electrostatic potentials. Changes in electrostatic potential from negative to positive are seen in transition from blue to red. As shown in Fig. 6, A and B, the pyrazole and lactone rings had opposite electron density profiles. This finding suggests that the heterocyclic ring in rofecoxib is more electropositive than the heterocyclic ring in celecoxib.

On the basis of this computer modeling data, we attempted to alter the surface potential of rofecoxib to mimic that of celecoxib by repositioning the lactone carbonyl group in the opposite orientation (Fig. 6, C). The total electrostatic potential map of the resulting isomer, compound **47,** was similar to that of celecoxib (Fig. 6, A versus C). However, because compound **47,** which contained a methylsulfone group, showed poor activity in eliciting apoptosis in PC-3 cells (apoptosis index, –) (data not shown), we also modeled the surface electrostatic potentials of

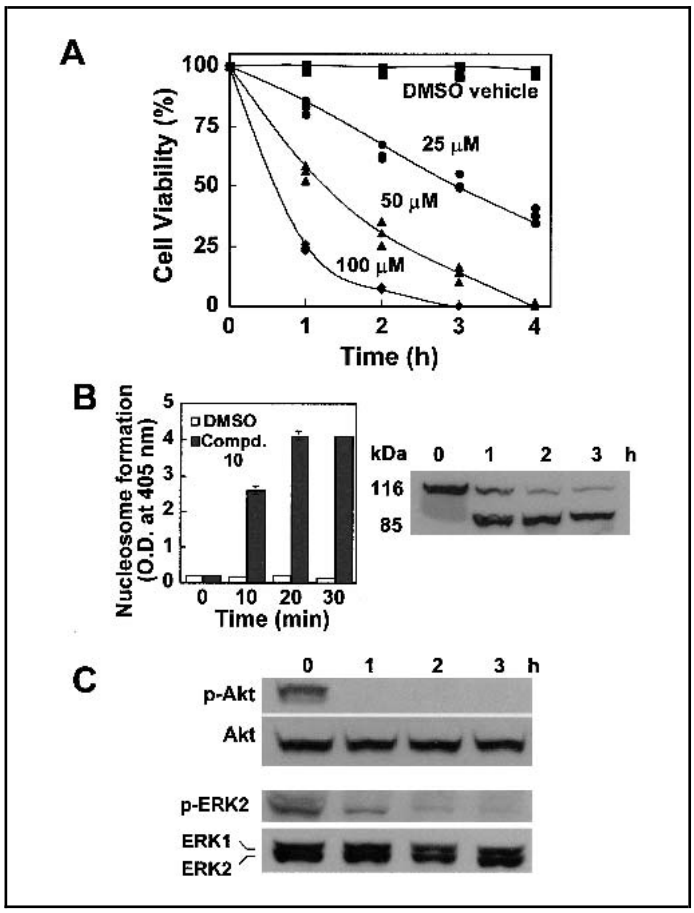

Fig. 4. Induction of apoptosis in PC-3 cells by compound **10.** **A**) Time- and dose-dependent effects of compound **10** on the cell viability of PC-3 cells in serum-free RPMI-1640 medium. Values obtained from three replicates were plotted for each time point at the indicated concentration of compound **10.** Control PC-3 cells were treated with a dimethyl sulfoxide (DMSO) vehicle. **B**) Evidence of apoptotic death in compound **10**-treated PC-3 cells. **Left panel,** time course of the formation of cytoplasmic nucleosomal DNA in PC-3 cells treated with DMSO vehicle or compound **10** (50 μ*M*). The formation of cytoplasmic nucleosomal DNA was quantitatively measured by a cell death detection enzyme-linked immunosorbent assay with lysates equivalent to 10^4 cells for each assay. Data are presented as means; **error bars** represent 95% confidence intervals (n = 3). **Right panel,** induction of poly(ADP-ribose) polymerase (PARP) cleavage by compound **10** in PC-3 cells. PC-3 cells were treated with 50 μ*M* compound **10** for the indicated times. PARP proteolysis to the apoptosis-specific 85-kd fragment was monitored by western blotting. O.D. = optical density. **C**) Time-dependent effects of 50 μ*M* compound **10** on Akt and ERK2 phosphorylation. PC-3 cells were treated with 50 μ*M* compound **10** for the indicated times and lysed, and proteins in the resulting supernatants were resolved on sodium dodecyl sulfate–polyacrylamide gels and subjected to western blot analysis. The phosphorylation status of Akt and ERK2 was determined by immunoblotting with the respective phospho-specific antibodies. Unphosphorylated Akt and ERK2, as immunostained by anti-Akt and anti-ERK2 antibodies, were used as internal standards for the comparison of phospho-Akt and phospho-ERK2 levels among samples of different exposure intervals. The blots are representative of three independent experiments. p-Akt = phosphorylated Akt; p-ERK2 = phosphorylated ERK2.

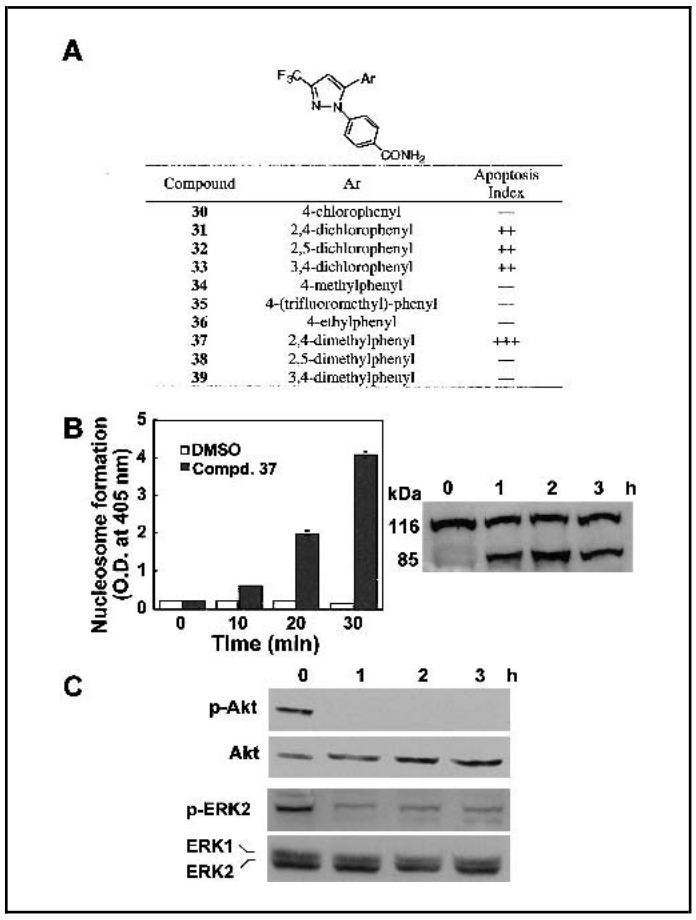

Compound	Ar	Apoptosis Index
30	4-chlorophenyl	—
31	2,4-dichlorophenyl	++
32	2,5-dichlorophenyl	++
33	3,4-dichlorophenyl	++
34	4-methylphenyl	—
35	4-(trifluoromethyl)-phenyl	—
36	4-ethylphenyl	—
37	2,4-dimethylphenyl	+++
38	2,5-dimethylphenyl	—
39	3,4-dimethylphenyl	—

Fig. 5. Effect of carboxamide derivatives on apoptosis in PC-3 cells. **A**) Activities of compounds **30**–**39** in inducing apoptosis in PC-3 cells. The general structure of these molecules is shown at the top. PC-3 cells were exposed to the test agent (50 μ*M*) in serum-free RPMI-1640 medium. Ar represents different aromatic ring structures contained on the compounds. The apoptosis index was determined as described in the "Materials and Methods" section. The cell viability was analyzed by trypan blue dye exclusion assay. **B**) Evidence for apoptotic death in compound **37**-treated PC-3 cells. **Left panel,** time course of the formation of cytoplasmic nucleosomal DNA in PC-3 cells treated with dimethyl sulfoxide (DMSO) vehicles or compound **37** (50 μ*M*) [ANOVA, $P<.001$; treated versus DMSO at 10, 20, and 30 minutes]. Data are presented as the mean values of three experiments; **bars** represent 95% confidence intervals. **Right panel,** induction of poly(ADP-ribose) polymerase cleavage by compound **37** in PC-3 cells. **C**) Time-dependent effect of 50 μ*M* compound **37** on Akt and ERK2 phosphorylation. The blots are representative of three independent experiments. All of the above experiments were carried out in a manner similar to that described for Fig. 4.

the corresponding sulfonamide-containing compound, compound **48,** and its dichloro- analogues, compounds **49** and **50.** Compound **49,** which had a substantially higher apoptosis index ($T_{50\%}$ at 50 μ*M* = 15 hours; apoptosis index, +) than rofecoxib, compound **48,** or compound **50** (each of which showed no appreciable apoptosis induction at 24 hours; apoptosis index, – [data not shown]), had an electrostatic potential map that strongly resembled that of its pyrazole counterpart, compound **8** (apoptosis index, +++) (Fig. 3). In addition, the similarity in the electrostatic potential profile of compound **49** and compound **8** (Fig. 6, D and E) was akin to the similarity in the profiles of celecoxib and compound **47,** but improved on the 5-aryl moiety. These data demonstrate that a clear understanding of the stereoelectronic characteristics of the entire conjugated system may provide a novel way of associating structural changes with the apoptosis-inducing activities of these compounds.

Discussion

Our previous demonstration that the effects of COX-2 inhibitors on apoptosis were distinct from their effects on COX-2 inhibition *(25)* suggested that effects on signaling targets other than COX-2, i.e., those involved in apoptosis, could be pharma-

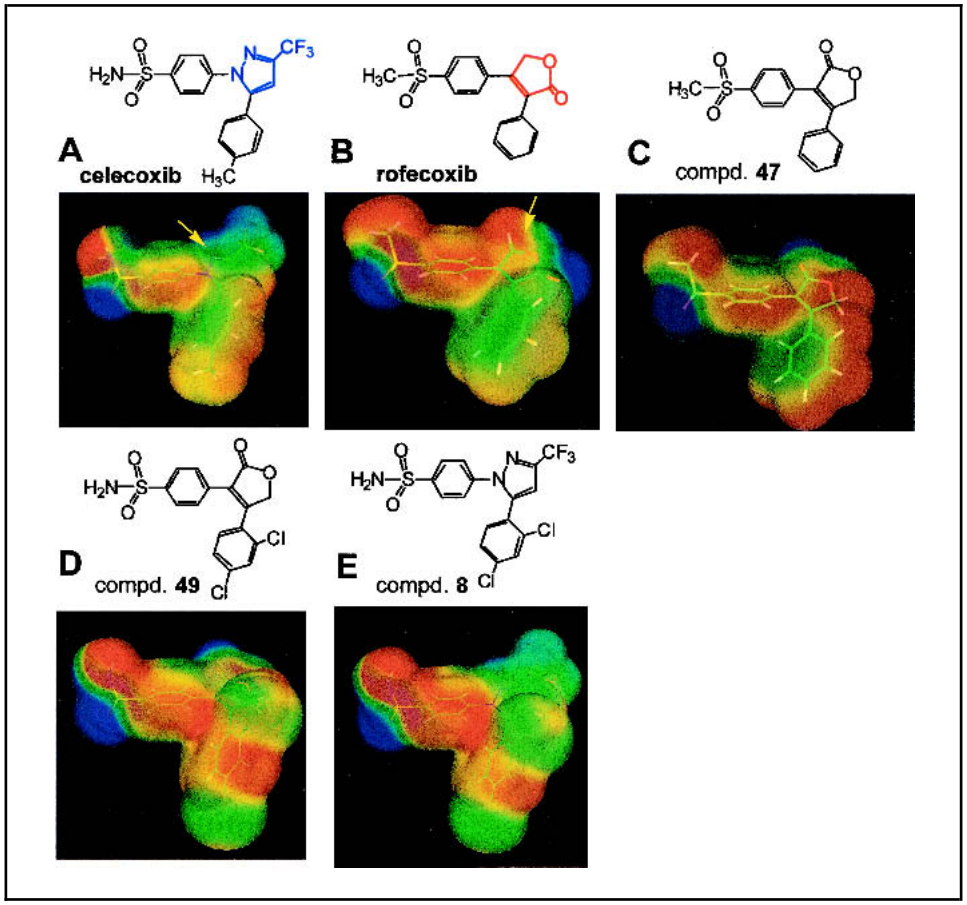

Fig. 6. Molecular modeling of celecoxib (**A**), rofecoxib (**B**), compound **47** (**C**), compound **49** (**D**), and compound **8** (**E**). The electrostatic potential of individual areas is coded in color: **blue** and **red** denote negative and positive electrostatic potentials, respectively. The pyrazole and lactone rings of celecoxib (**panel A**) and rofecoxib (**panel B**) were colored **blue** and **red,** respectively, in the chemical structures and indicated by **arrows** in the electrostatic potential images. Other colors, such as green and yellow, reflect transitions between negative and positive electrostatic potentials (and vice versa).

cologically exploited to generate novel apoptosis-inducing agents. This study was thus aimed at identifying the key structural elements of the COX-2 inhibitor celecoxib that contribute to its apoptosis-inducing activity in human prostate cancer cells. On the basis of our structure–function data, we propose a working model that outlines the structural features essential for the apoptotic effects of celecoxib (Fig. 7).

We found that the structural requirements for apoptosis induction are different from those for COX-2 inhibition. In particular, the induction of apoptosis in PC-3 cells by compounds derived from COX-2 inhibitors had stringent requirements with regard to the heterocyclic system and the amide moiety (in the form of sulfonamide or carboxamide groups). These structural features highlight the potential importance of surface electrostatic potential and hydrogen bonding for interactions between these compounds and the protein target(s), and they may account for the discrepancy in the apoptosis-inducing activities of celecoxib and the other COX-2 inhibitors we examined. We also found that apolar substituents at the terminal phenyl function had a profound effect in that enlargement of the hydrophobic aryl group of celecoxib enhanced the apoptosis-inducing activity of the resulting compound. This flexibility in functionality is in sharp contrast to the strict requirements necessary to maintain good COX-2 inhibitory activity *(29).* This model was validated by our structure–function data for converting rofecoxib to compound **49.** Computer modeling analysis of celecoxib versus rofecoxib suggested a link between the surface electrostatic potential surrounding the heterocyclic system and apoptosis-inducing potency. A comparison of the surface electrostatic potentials of celecoxib (apoptosis index, ++) and rofecoxib (apoptosis index, −) revealed important differences in electron density. We therefore modified the structure of rofecoxib to approximate the surface electrostatic potential of celecoxib, which resulted in the design of structural variants compounds **47**–**50.** Among the variants, compound **49** showed a substantial increase in apoptosis-inducing activity.

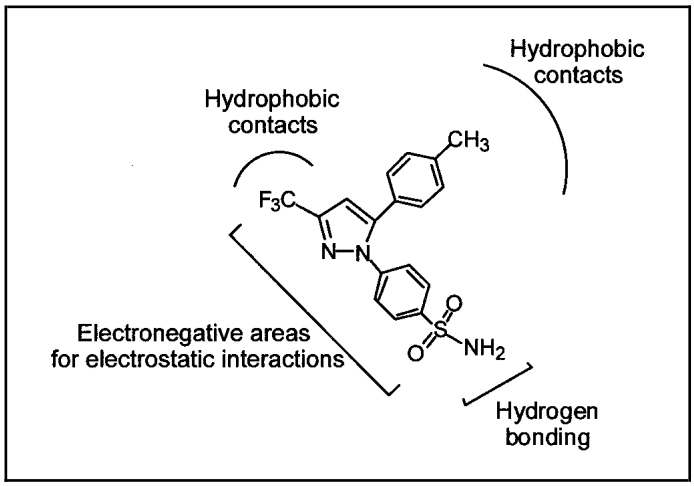

Fig. 7. A working model outlining the structural features essential for the apoptotic effect of celecoxib.

Our statistical analysis of data from three different prostate cancer cell lines suggests that the induction of apoptosis by the active compounds was not dependent on androgen sensitivity, p53 functional status, or the level of Bcl-2 expression. The effectiveness of these agents against androgen-independent pros-

tate cancer (i.e., PC-3) cells is especially noteworthy. Metastatic prostate cancers are lethal because they are heterogeneously composed of both androgen-dependent and androgen-independent malignant cells *(35,36).* Because androgen-independent prostate cancer cells are resistant to the induction of apoptosis by androgen ablative therapy, an important strategy in developing effective chemotherapy for metastatic prostate cancer is to specifically eliminate androgen-independent cells by targeted apoptosis *(35,36).* The apoptotic action of these celecoxib derivatives against androgen-independent prostate cancer cells underscores their unique signaling mechanism in disrupting multiple signaling pathways (i.e., Akt and ERK2) that are essential to cancer cell survival *(26,27).*

In addition to its effects on apoptosis induction, celecoxib has effects on angiogenesis *(37–40).* It has been reported that celecoxib suppresses corneal blood vessel formation in a rat model via a COX-2-dependent mechanism *(38).* However, our preliminary data indicate that celecoxib derivatives that can induce apoptosis in prostate cancer cells but that lack COX-2 inhibitory activity can also inhibit angiogenesis in the yolk sac of chicken embryos, with potencies comparable with or higher than that of celecoxib (Kulp S, Lin H, Zhu J, Ward P, Chen K, and Chen C: unpublished results). This finding suggests that the anti-angiogenic activity of celecoxib may, in part, be attributable to a COX-2-independent pathway. In view of the crucial role of Akt and ERK2 signaling in embryonal angiogenesis *(41),* it is possible that the anti-angiogenic effects of celecoxib and its derivatives are mediated through a mechanism similar to the one that induces apoptosis, i.e., Akt and ERK2 dephosphorylation.

It is important to note that, when given at therapeutic doses (oral administration of 400–800 mg per day), celecoxib reaches peak plasma concentrations of 3–8 μM *(42),* severalfold lower than the concentrations required to induce apoptosis in prostate cancer cells in serum-free medium (i.e., 25 μM or higher). It is conceivable that the observed *in vivo* antitumor activity of celecoxib may arise from the concerted action of multiple mechanisms that include both the induction of apoptosis and the inhibition of angiogenesis. Consequently, our current research focuses on discerning the relative contributions of these mechanisms to the *in vivo* effects of celecoxib and its derivatives on tumor growth. In addition, investigations of the pharmacokinetic, pharmacodynamic, and toxicity profiles of these apoptosis-inducing agents are under way.

REFERENCES

(1) Peleg II, Wilcox CM. The role of eicosanoids, cyclooxygenases, and nonsteroidal anti-inflammatory drugs in colorectal tumorigenesis and chemoprevention. J Clin Gastroenterol 2002;34:117–25.

(2) Krishnan K, Brenner DE. Prostaglandin inhibitors and the chemoprevention of noncolonic malignancy. Gastroenterol Clin North Am 2001;30: 981–1000.

(3) Vainio H. Is COX-2 inhibition a panacea for cancer prevention? Int J Cancer 2001;94:613–4.

(4) Sjodahl R. Nonsteroidal anti-inflammatory drugs and the gastrointestinal tract. Extent, mode, and dose dependence of anticancer effects. Am J Med 2001;110:66S–69S.

(5) Lynch PM. COX-2 inhibition in clinical cancer prevention. Oncology (Huntingt) 2001;15:21–6.

(6) Castelao JE, Yuan JM, Gago-Dominguez M, Yu MC, Ross RK. Nonsteroidal anti-inflammatory drugs and bladder cancer prevention. Br J Cancer 2000;82:1364–9.

(7) Harris RE, Alshafie GA, Abou-Issa H, Seibert K. Chemoprevention of breast cancer in rats by celecoxib, a cyclooxygenase 2 inhibitor. Cancer Res 2000;60:2101–3.

(8) Fournier DB, Gordon GB. COX-2 and colon cancer: potential targets for chemoprevention. J Cell Biochem 2000;77:97–102.

(9) Nelson JE, Harris RE. Inverse association of prostate cancer and nonsteroidal anti-inflammatory drugs (NSAIDs): results of a case-control study. Oncol Rep 2000;7:169–70.

(10) Shiff SJ, Rigas B. The role of cyclooxygenase inhibition in the antineoplastic effects of nonsteroidal antiinflammatory drugs (NSAIDs). J Exp Med 1999;190:445–50.

(11) Patrignani P. Nonsteroidal anti-inflammatory drugs, COX-2 and colorectal cancer. Toxicol Lett 2000;112–113:493–8.

(12) Prescott SM, Fitzpatrick FA. Cyclooxygenase-2 and carcinogenesis. Biochim Biophys Acta 2000;1470:M69–78.

(13) Dempke W, Rie C, Grothey A, Schmoll HJ. Cyclooxygenase-2: a novel target for cancer chemotherapy? J Cancer Res Clin Oncol 2001;127:411–7.

(14) Sheng H, Shao J, Morrow JD, Beauchamp RD, DuBois RN. Modulation of apoptosis and Bcl-2 expression by prostaglandin E2 in human colon cancer cells. Cancer Res 1998;58:362–6.

(15) Zhang Z, DuBois RN. Par-4, a proapoptotic gene, is regulated by NSAIDs in human colon carcinoma cells. Gastroenterology 2000;118:1012–7.

(16) McGinty A, Chang YW, Sorokin A, Bokemeyer D, Dunn MJ. Cyclooxygenase-2 expression inhibits trophic withdrawal apoptosis in nerve growth factor-differentiated PC12 cells. J Biol Chem 2000;275:12095–101.

(17) Oshima M, Dinchuk JE, Kargman SL, Oshima H, Hancock B, Kwong E, et al. Suppression of intestinal polyposis in Apc delta716 knockout mice by inhibition of cyclooxygenase 2 (COX-2). Cell 1996;87:803–9.

(18) Hawk ET, Viner JL, Dannenberg A, DuBois RN. COX-2 in cancer—a player that's defining the rules. J Natl Cancer Inst 2002;94:545–6.

(19) Marx J. Cancer research. Anti-inflammatories inhibit cancer growth—but how? Science 2001;291:581–2.

(20) Piazza GA, Rahm AL, Krutzsch M, Sperl G, Paranka NS, Gross PH, et al. Antineoplastic drugs sulindac sulfide and sulfone inhibit cell growth by inducing apoptosis. Cancer Res 1995;55:3110–6.

(21) Lim JT, Piazza GA, Han EK, Delohery TM, Li H, Finn TS, et al. Sulindac derivatives inhibit growth and induce apoptosis in human prostate cancer cell lines. Biochem Pharmacol 1999;58:1097–107.

(22) Thompson HJ, Jiang C, Lu J, Mehta RG, Piazza GA, Paranka NS, et al. Sulfone metabolite of sulindac inhibits mammary carcinogenesis. Cancer Res 1997;57:267–71.

(23) Thompson WJ, Piazza GA, Li H, Liu L, Fetter J, Zhu B, et al. Exisulind induction of apoptosis involves guanosine 3′,5′-cyclic monophosphate phosphodiesterase inhibition, protein kinase G activation, and attenuated beta-catenin. Cancer Res 2000;60:3338–42.

(24) Haanen C. Sulindac and its derivatives: a novel class of anticancer agents. Curr Opin Investig Drugs 2001;2:677–83.

(25) Song X, Lin HP, Johnson AJ, Tseng PH, Yang YT, Kulp SK, et al. Cyclooxygenase-2, player or spectator in cyclooxygenase-2 inhibitor-induced apoptosis in prostate cancer cells. J Natl Cancer Inst 2002;94:585–91.

(26) Hsu AL, Ching TT, Wang DS, Song X, Rangnekar VM, Chen CS. The cyclooxygenase-2 inhibitor celecoxib induces apoptosis by blocking Akt activation in human prostate cancer cells independently of Bcl-2. J Biol Chem 2000;275:11397–403.

(27) Johnson AJ, Song X, Hsu A, Chen C. Apoptosis signaling pathways mediated by cyclooxygenase-2 inhibitors in prostate cancer cells. Adv Enzyme Regul 2001;41:221–35.

(28) Li JJ, Norton MB, Reinhard EJ, Anderson GD, Gregory SA, Isakson PC, et al. Novel terphenyls as selective cyclooxygenase-2 inhibitors and orally active anti-inflammatory agents. J Med Chem 1996;39:1846–56.

(29) Penning TD, Talley JJ, Bertenshaw SR, Carter JS, Collins PW, Docter S, et al. Synthesis and biological evaluation of the 1,5-diarylpyrazole class of cyclooxygenase-2 inhibitors: identification of 4-[5-(4-methylphenyl)-3-(trifluoromethyl)-1H-pyrazol-1-yl]benzenesulfonamide (SC-58635, celecoxib). J Med Chem 1997;40:1347–65.

(30) Talley JJ, Brown DL, Carter JS, Graneto MJ, Koboldt CM, Masferrer JL, et al. 4-[5-Methyl-3-phenylisoxazol-4-yl]-benzenesulfonamide, valdecoxib: a potent and selective inhibitor of COX-2. J Med Chem 2000;43: 775–7.

(31) Puig C, Crespo MI, Godessart N, Feixas J, Ibarzo J, Jimenez JM, et al. Synthesis and biological evaluation of 3,4-diaryloxazolones: a new class of orally active cyclooxygenase-2 inhibitors. J Med Chem 2000;43: 214–23.

(32) Frisch MJ, Trucks GW, Schlegel HB, Scuseria GE, Robb MA, Cheeseman JR, et al. Gaussian 98 (Revision A7). Pittsburg (PA): Gaussian, Inc.; 1998.
(33) Laaksonen L. A graphics program for the analysis and display of molecular dynamics trajectories. J Mol Graph 1992;10:33–4.
(34) Bergman DL, Laaksonen L, Laaksonen A. Visualization of solvation structures in liquid mixtures. J. Mol Graph Model 1997;15:301–6, 328–33.
(35) Laufer M, Denmeade SR, Sinibaldi VJ, Carducci MA, Eisenberger MA. Complete androgen blockade for prostate cancer: what went wrong? J Urol 2000;164:3–9.
(36) Isaacs JT. Apoptosis: translating theory to therapy for prostate cancer. J Natl Cancer Inst 2000;92:1367–9.
(37) Jones MK, Wang H, Peskar BM, Levin E, Itani RM, Sarfeh IJ, et al. Inhibition of angiogenesis by nonsteroidal anti-inflammatory drugs: insight into mechanisms and implications for cancer growth and ulcer healing. Nat Med 1999;5:1418–23.
(38) Masferrer JL, Leahy KM, Koki AT, Zweifel BS, Settle SL, Woerner BM, et al. Antiangiogenic and antitumor activities of cyclooxygenase-2 inhibitors. Cancer Res 2000;60:1306–11.
(39) Szabo IL, Pai R, Soreghan B, Jones MK, Baatar D, Kawanaka H, et al. NSAIDs inhibit the activation of egr-1 gene in microvascular endothelial cells. A key to inhibition of angiogenesis? J Physiol Paris 2001;95:379–83.
(40) Leahy KM, Ornberg RL, Wang Y, Zweifel BS, Koki AT, Masferrer JL. Cyclooxygenase-2 inhibition by celecoxib reduces proliferation and induces apoptosis in angiogenic endothelial cells in vivo. Cancer Res 2002; 62:625–31.
(41) Jiang BH, Zheng JZ, Aoki M, Vogt PK. Phosphatidylinositol 3-kinase signaling mediates angiogenesis and expression of vascular endothelial growth factor in endothelial cells. Proc Natl Acad Sci U S A 2000;97: 1749–53.
(42) Davies NM, McLachlan AJ, Day RO, Williams KM. Clinical pharmacokinetics and pharmacodynamics of celecoxib: a selective cyclooxygenase-2 inhibitor. Clin Pharmacokinet 2000;38:225–42.

NOTES

Supported by Public Health Service grants CA92307 and CA94829 from the National Cancer Institute (NCI), National Institutes of Health (NIH), Department of Health and Human Services (DHHS); by Army grant DAMD17-02-1-0117 (to C.-S. Chen); and by grant P30 CA16058 from the NCI, NIH, DHHS (to the Comprehensive Cancer Center, The Ohio State University).

Manuscript received March 11, 2002; revised August 27, 2002; accepted September 19, 2002.